Specificity of Phosphorylation Responses to Mitogen Activated Protein (MAP) Kinase Pathway Inhibitors in Melanoma Cells*[S]

Joel Basken‡, Scott A. Stuart‡, Andrew J. Kavran‡§, Thomas Lee‡, Christopher C. Ebmeier¶, William M. Old¶, and Natalie G. Ahn‡§‖

The BRAF-MKK1/2-ERK1/2 pathway is constitutively activated in response to oncogenic mutations of BRAF in many cancer types, including melanoma. Although small molecules that inhibit oncogenic BRAF and MAP kinase kinase (MKK)1/2 have been successful in clinical settings, resistance invariably develops. High affinity inhibitors of ERK1/2 have been shown in preclinical studies to bypass the resistance of melanoma and colon cancer cells to BRAF and MKK1/2 inhibitors, and are thus promising additions to current treatment protocols. But still unknown is how molecular responses to ERK1/2 inhibitors compare with inhibitors currently in clinical use. Here, we employ quantitative phosphoproteomics to evaluate changes in phosphorylation in response to the ERK inhibitors, SCH772984 and GDC0994, and compare these to the clinically used MKK1/2 inhibitor, trametinib. Combined with previous studies measuring phosphoproteomic responses to the MKK1/2 inhibitor, selumetinib, and the BRAF inhibitor, vemurafenib, the outcomes reveal key insights into pathway organization, phosphorylation specificity and off-target effects of these inhibitors. The results demonstrate linearity in signaling from BRAF to MKK1/2 and from MKK1/2 to ERK1/2. They identify likely targets of direct phosphorylation by ERK1/2, as well as inhibitor off-targets, including an off-target regulation of the p38α mitogen activated protein kinase (MAPK) pathway by the MKK1/2 inhibitor, trametinib, at concentrations used in the literature but higher than *in vivo* drug concentrations. In addition, several known phosphorylation targets of ERK1/2 are insensitive to MKK or ERK inhibitors, revealing variability in canonical pathway responses between different cell systems. By comparing multiple inhibitors targeted to multiple tiers of protein kinases in the MAPK pathway, we gain insight into regulation and new targets of the oncogenic BRAF driver pathway in cancer cells, and a useful approach for evaluating the specificity of drugs and drug candidates. ***Molecular & Cellular Proteomics 17: 10.1074/mcp.RA117.000335, 550–564, 2018.***

The mitogen activated protein (MAP)[1] kinase cascade (BRAF-MKK1/2-ERK1/2) is constitutively activated in many cancer types, including melanoma, colorectal, thyroid, and ovarian cancers (1). Up-regulation of this pathway is particularly important in melanoma, where as many as 50% of cases display oncogenic mutations in BRAF (V600E/K), and 20% display oncogenic mutations in NRAS (2). Therapeutics that specifically target oncogenic BRAF and its downstream substrates MAP kinase kinase (MKK)1/2 (*aka* MEK1/2) have been successful in both clinical and preclinical settings. To date, two MKK1/2 inhibitors (trametinib and cobimetinib) and two mutant BRAF inhibitors (vemurafenib and dabrafenib) (3, 4) are FDA-approved as single agent or combination drug therapies. These inhibitors can elicit dramatic responses in patients, and combination treatments using BRAF and MKK1/2 inhibitors are now first-line therapies for treating metastatic melanomas harboring oncogenic BRAF mutations.

A previous phosphoproteomics study from our lab compared molecular responses to the BRAF inhibitor, vemurafinib, and MKK1/2 inhibitor, selumetinib, and demonstrated nearly complete overlap in pathway targets (5). This suggests that mitogen activated protein kinase (MAPK) pathway signaling at the level of BRAF and MKK1/2 works in a predominantly linear manner, with little evidence for bifurcation in the path-

From the ‡Department of Chemistry and Biochemistry, §BioFrontiers Institute, ¶Department of Molecular, Cellular, Developmental Biology, University of Colorado, Boulder, CO 80303

Received September 16, 2017, and in revised form, November 8, 2017

Published, MCP Papers in Press, December 18, 2017, DOI 10.1074/mcp.RA117.000335

Author contributions: J.B., S.A.S., and N.G.A. designed research; J.B. performed research; J.B., S.A.S., A.J.K., W.O., and N.G.A. analyzed data; J.B., S.A.S., and N.G.A. wrote the paper; T.L. and C.C.E. ran MS samples.

[1] The abbreviations used are: MAP, mitogen activated protein; AGC, automatic gain control; DAVID, database for annotation, visualization and integrated discovery; DEF, docking site for ERK – FXF; DEJL, docking site for ERK and JNK – LXL; ERK, extracellular signal related kinase; ERLIC, electrostatic repulsion-hydrophilic interaction chromatography; FASP, filter assisted sample preparation; FDR, false discovery rate; FTMS, Fourier transform mass spectrometry; GDC, GDC0994; ITMS, ion trap mass spectrometry; LTQ, linear trap quadrupole; MAPK, mitogen activated protein kinase; MKK, MAP kinase kinase (*aka* MAP/ERK kinase; MEK); SCH, SCH772984; SEL, selumetinib; SILAC, stable isotope labeling by amino acids in cell culture; TiO_2, titanium dioxide; TRA, trametinib; UPLC, ultra performance liquid chromatography.

way upstream of MKK1/2. Consistent with this finding, combining these inhibitors at subsaturating concentrations elicited responses that were almost invariably additive (5). This suggests that BRAF and MKK1/2 inhibitors in combination may be more effective than treatment with a single inhibitor because of their additive effects on ERK1/2 inhibition, and that incomplete ERK1/2 inhibition at maximally tolerated doses may limit the efficacy of single drugs and possibly combination therapies.

Despite the high response rates to combination therapies in mutant BRAF-positive patients, resistance invariably develops, usually through mechanisms that reactivate MAPK signaling even in the presence of drug (6). Importantly, in preclinical studies of cultured cells and xenograft tumors, cancer cells resistant to BRAF or MKK1/2 inhibitors are nevertheless sensitive to high affinity inhibitors of ERK1/2 (7, 8). Therefore, development of ERK1/2 inhibitors is a promising strategy to combat resistance, and several compounds are currently in early stage clinical trials (7). Addition of ERK1/2 inhibitors to treatment strategies may provide an effective way to extend progression-free survival in patients. Therefore, understanding the molecular responses to ERK1/2 inhibitors and comparing these to clinically used BRAF and MKK1/2 inhibitors are important for maximizing their effectiveness.

An unanswered question is the degree to which inhibitors of ERK1/2 and MKK1/2 target the same molecular responses. Here we use phosphoproteomics to compare the responses of the ERK1/2 inhibitors, SCH772984 and GDC0994, and the clinically used MKK1/2 inhibitor, trametinib, in human metastatic melanoma cells. These are compared with responses to the MKK1/2 inhibitor, selumetinib, previously measured in our lab in the same melanoma cell line. Direct comparisons between SCH772984 and trametinib demonstrate strong correlations in responses at individual phosphosites, revealing that MAPK signaling is predominantly linear between MKK1/2 and ERK1/2, with few if any points of bifurcation upstream of ERK1/2. Phosphosites inhibited in common by all four MKK1/2 or ERK1/2 inhibitors are highly likely to be regulated by the MAPK pathway. From these, we identify new candidates for phosphorylation by ERK1/2. In contrast, phosphosites unique to a single inhibitor most likely reflect off-target effects of each compound. Notably, trametinib uniquely inhibits regulatory phosphorylation sites on p38α MAPK, and blocks the activation of this kinase in response to osmotic stress. We show that this is because of the ability of trametinib to inhibit MKK6, an effect not observed with selumetinib. A comparison between all four inhibitors reveals the most off-target effects with GDC0994, and fewer with trametinib, selumetinib or SCH772984. Comparison of all inhibitors also reveals a subset of validated ERK targets which appear refractory to regulation by the BRAF-MKK-ERK pathway in our system. Taken together, the strategy of using phosphoproteomics to evaluate inhibitors against multiple tiers of the MAP kinase cascade can be useful for revealing pathway linearity and identifying new pathway targets, as well as evaluating off-target effects of inhibitors and variability in signaling responses between different cell systems. They provide new characterizations of ERK1/2 inhibitors which are under development for cancer treatment to improve clinical responses to BRAF and MKK inhibitors.

EXPERIMENTAL PROCEDURES

Cell Culture—WM239A metastatic melanoma cells were a kind gift of Dr. Meenhard Herlyn, Wistar Institute, Philadelphia PA. Cells were SILAC-labeled using SILAC RPMI media (Thermo Fisher Scientific, Waltham, MA, 89984) supplemented with isotopically-labeled heavy (H), medium (M), or light (L)-Arg (40 μg/ml) and -Lys (200 μg/ml) (Cambridge Isotope Laboratories, Tewksbury, MA), in addition to unlabeled Pro (180 μg/ml, Sigma-Aldrich, St. Louis, MO, P0380), 10% (v/v) dialyzed FCS (Life Technologies, Carlsbad, CA, 88440), penicillin (100 μg/ml, Thermo Fisher Scientific), and streptomycin (100 μg/ml, Thermo Fisher Scientific). Non-SILAC experiments used cells cultured in Gibco RPMI 1640 media (2400–089) and 10% FCS, with or without penicillin-streptomycin. Cells were incubated in a humidified chamber maintained at 37 °C with 5% CO_2. Inhibitors used were trametinib (Selleck, Houston, TX), SCH772984 (Selleck), and GDC0994 (Selleck).

Experimental Design and Statistical Rationale—To directly compare phosphoproteomic responses to trametinib and SCH772984 in WM239A cells, triple labeled SILAC experiments were performed in three biological replicates. DMSO carrier was used as a negative control, and isotopic labels for each treatment were varied between each replicate, to control for isotope effects. A similar experimental design was used to directly compare cell responses to GDC0994 and SCH772984 against DMSO carrier.

Sample Preparation—WM239A cells grown in H-, M- or L-Arg/Lys SILAC RPMI were plated in 150 mm dishes (35×10^6 cells/dish). The following day, each dish was treated with inhibitor (10 μM) or DMSO for 2 h. Lysates (8 mg) from each H-, M- and L-labeled dish were then mixed (24 mg total) and proteolyzed with trypsin (Promega, Madison, WI, 0.5 mg, 2% w/w), and phosphopeptides were enriched with TiO_2 (GL Sciences, Torrance, CA, 5 μm, 240 mg) and fractionated by ERLIC chromatography (PolyLC, Columbia, MD, 100 $\times$ 4.6 mm 5 μm polyWAX LP) as previously described (5). Nonenriched tryptic peptides sampled prior to TiO_2 were fractionated with an M-class Acquity UPLC (Waters, Milford, MA), using a reverse-phase C18 column prepared in-house (UChrom 1.8 μm 120Å, 0.5 mm i.d. $\times$ 200 mm) equilibrated in 10 mM ammonium formate, pH 10, and eluted with a 5–80% linear gradient of acetonitrile over 170 min.

Mass Spectrometry—For SILAC experiments comparing DMSO, trametinib and SCH772984, LC-MS/MS analysis was performed with an Orbitrap Fusion (Thermo Scientific) using either a nanoLC1000 (Thermo Scientific) or an M-class Acquity (Waters) UPLC. ERLIC fractions of TiO_2-enriched phosphopeptides were loaded directly onto a Peptide BEH C18 column (1.7 μm 130Å, 75 μm $\times$ 250 mm, Acquity M-class, Waters) equilibrated in 0.1% formic acid and eluted with a gradient from 3–20% acetonitrile in 100 min, 20–32% acetonitrile in 20 min, 32–85% acetonitrile in 1 min, and holding at 85% for 4 min. MS scans (380–1500 *m/z*) were collected with resolution of 120,000, AGC target of 2×10^5, and a maximum inject fill time of 50 ms. MS/MS scans were acquired by HCD fragmentation, using top speed mode for 3 s on the most intense ions with a quadrupole isolation window of 1.6 Da and normalized collision energy of 35%. Fragment ions were collected in either the Orbitrap (replicates 1,3) or the linear ion trap (replicate 2). Total proteins were analyzed by LC-MS/MS of peptides not enriched by TiO_2 using the same instrument settings. For SILAC experiments comparing DMSO, SCH772984,

and GDC0994, LC-MS/MS was performed with a LTQ Orbitrap Velos mass spectrometer and Waters Acquity UPLC, using gradient elution and instrument settings previously described (5).

Data and Statistical Analysis—Raw MS files for phosphopeptide and total peptide fractions were analyzed together using the Andromeda search engine in MaxQuant v1.5.4.2 (9) software and processed with Perseus software (v1.5.4.2) using default settings as described (5). MaxQuant identifies common contaminants and peptides matching to a target-decoy database containing reversed versions of each peptide in the uploaded Uniprot database. The previously published DMSO-selumetinib-vemurafenib data set (5) was also reprocessed with these software versions. Searches used the Uniprot human proteome reference (08/21/2015 download, with 21,051 entries). Mass tolerances were 20 ppm for FTMS precursor ions and 0.5 Da for ITMS MS/MS ions. The minimum peptide length was 7 amino acids. MaxQuant default score cutoffs of 0 for unmodified peptides and 40 for modified peptides were used. False discovery rates were 1% for both phosphopeptide and protein identifications. For protein quantification, the minimum number of total peptides was 2 (unique + razor). Phosphorylated peptides and their unmodified counterparts were excluded for protein quantification. Raw files for phosphopeptide data and total protein data were defined as separate groups. Multiplicity was set to 3 with medium labels of Arg6 and Lys4 and heavy labels of Arg10 and Lys8 for both groups. All files were searched with carbamidomethylation (Cys) as a fixed modification and acetylation (N-term) and oxidation (Met) as variable modifications. The enzyme specificity was trypsin/P and up to two missed cleavages were allowed. For phosphopeptide files, Phospho(STY) was set as a variable modification, and phosphate localization probabilities were assessed with the MaxQuant PTM score. Localization probabilities less than 0.75 were considered ambiguous site assignments. To report phosphopeptide data, the Phospho (STY)Sites output file was uploaded into Perseus. Reverse and contaminant rows were removed and the site table was expanded so that ratios for singly, doubly, and "triply" (*i.e.* 3 or more phosphates) phosphorylated peptides were treated as individual phosphosites. Rows not quantified in any of the experiments after expanding the site table were removed. For total peptide samples, the protein groups output file was uploaded into the Perseus and rows not quantified or designated as reverse, contaminant, and only identified by site were removed. The mass spectrometry proteomics data have been deposited to the ProteomeXchange Consortium (10) via the PRIDE partner repository with the data set identifier PXD007620 (DMSO-trametinib-SCH772984 SILAC experiment), PXD001560 (DMSO-selumetinib-vemurafenib SILAC experiment), and PXD007621 (DMSO-SCH772984-GDC0994 SILAC experiment).

Phosphopeptides with significant changes were accepted when quantified in two or three replicates and SILAC ratios exceeded an estimated average threshold of 1.8-fold ($\log_2 \pm 0.840$) using phosphosite-wise linear models in Bioconductor R package Limma v3.32.7 (11). We fit a linear model of the $\log_2$ ratios with DMSO as the reference treatment using the function lmFit. The contrasts were fit using the contrasts.fit function, and then moderated t-statistics were computed with the eBayes function. All functions used the default options. This threshold corresponds to FDR ≤ 0.01 ($|z\text{-score}| \geq 3.1$), which is greater than three standard deviations from the mean, as determined by a control experiment measuring SILAC ratios in a triple labeled experiment where each dish of labeled WM239A cells was treated with DMSO (5). To identify high-confidence phosphosites and control for variability among replicates, an empirical Bayesian analysis (eBayes function in Limma) was used to calculate adjusted *p* values controlling the false discovery rate (q-value) (12, 13). Phosphosites with FDR adjusted *p* values < 0.05 and average $|\log_2(\text{combined ratio})| \geq 0.84$ were deemed significant for subsequent analysis.

We compared the results of the DMSO-trametinib-SCH772984 SILAC experiment to our previous SILAC experiment which quantified phosphoproteomic responses to the MKK1/2 inhibitor selumetinib. To do this, we re-analyzed the raw files from (5) using MaxQuant v1.5.4.2 with the settings described above. Individual phosphosites were then matched based on identical 31 amino acid "sequence window" and "multiplicity" values from the MaxQuant Phospho (STY)Sites output files.

Immunoblotting—All antibodies used were from Cell Signaling Technology (Danvers, MA) and included anti-p38α (#9218), anti-phospho-p38 MAPK (#4511, Thr180/Tyr182), anti-β-tubulin (#2146), anti-ERK1/2 (#4696), anti-phospho-ERK1/2 (#4370, Thr202/Tyr204 and Thr185/Tyr187), anti-MKK1/2 (#4694), anti-phospho-MKK1/2 (#9154, Ser218/Ser222, and Ser222/Ser226), anti-phospho-p90RSK (#9335, Ser380), anti-MKK6 (#8550). Protein samples were separated on 7.5% or 10% SDS-PAGE and transferred to PVDF membranes (Immobilon-P-SQ, EMD Millipore, Billerica, MA), which were incubated with primary antibody overnight at 4 °C and secondary antibody for 1 h at room temperature. Pierce ECL2 substrate was used for immunoblot development using X-ray film and/or fluorescence imaging (Typhoon, GE Healthcare, Little Chalfont, UK).

Immunoprecipitation—After treating cells with DMSO or kinase inhibitors for 2 h, hyperosmotic stress was induced by adding a solution of 5 M NaCl + 0.4 M KCl to a final concentration of 181 mM NaCl and 12.5 mM KCl, yielding media with total osmolality of 500 mOsm/L. Cells were harvested in RIPA lysis buffer supplemented with cOmplete protease inhibitor and Phos-Stop phosphatase inhibitor cocktails (Roche, Basel, Switzerland), and lysate protein concentrations were determined using the BioRad DC protein assay (BioRad, Hercules, CA). Immunoprecipitation of p38α MAPK was carried out by incubating 250 μg cell lysate with 1 μg anti-p38α antibody overnight at 4 °C, followed by 20 μl Dynabeads Protein G (Thermo Fisher Scientific) for 1 h at 4 °C. Beads were collected magnetically, washed with cold phosphate-buffered saline (PBS) and incubated in Laemmli sample buffer for 10 min at 95 °C.

In Vitro Kinase Assays—Plasmids constructed in the lab of Roger Davis (14) were obtained from Addgene (Cambridge, MA): Flag-MKK6 (#13517), Flag-MKK6-S207E/T211E (#13518), and Flag-MKK6-K82A (#13519). Transfections (1×10^6 cells, 5 μg cDNA) were carried out by electroporation (NEON system, ThermoFisher Scientific) using 1200 V x 2 pulses X 20 ms/pulse. Cells were then incubated for 72 h followed by lysis in RIPA buffer. Flag-tagged proteins were purified using anti-Flag M2 affinity gel resin (Sigma-Aldrich), incubated with 300 μg lysate overnight at 4 °C. Resin was washed in cold Tris-buffered saline (TBS), resuspended in reaction buffer containing 10 mM $MgCl_2$, 1 mM ATP, 50 mM Tris-HCl pH 7.2, 50 mM NaCl and 1 mM dithiothreitol, and then incubated with DMSO or kinase inhibitor at room temperature for 15 min. Kinase reactions were initiated by adding 1 μg His_6-p38α MAPK, expressed in *E. coli* and purified by Ni-NTA and MonoQ chromatography as described (15). After 2 min at 30 °C, reactions were quenched by adding Laemmli sample buffer and heating at 95 °C for 10 min. Proteins were separated by SDS-PAGE followed by immunoblotting with anti-phospho-p38 MAPK. Reaction times and kinase amounts were chosen to ensure linearity of phosphorylation.

Cell Viability Assay—WM239A cells were seeded into 96-well dishes at 5000 cells per well and allowed to adhere for 4 h before treating with DMSO or varying concentrations of kinase inhibitor. After 72 h, cells were quantified using the CellTiter Glo 2.0 Assay (Promega) according to the manufacturer's protocol. Luminescence was recorded using a Biotek Synergy H1 plate reader (Biotek Instruments, Winooski, VT) and curve-fitting was done using Origin software (OriginLab Corp., Northampton, MA).

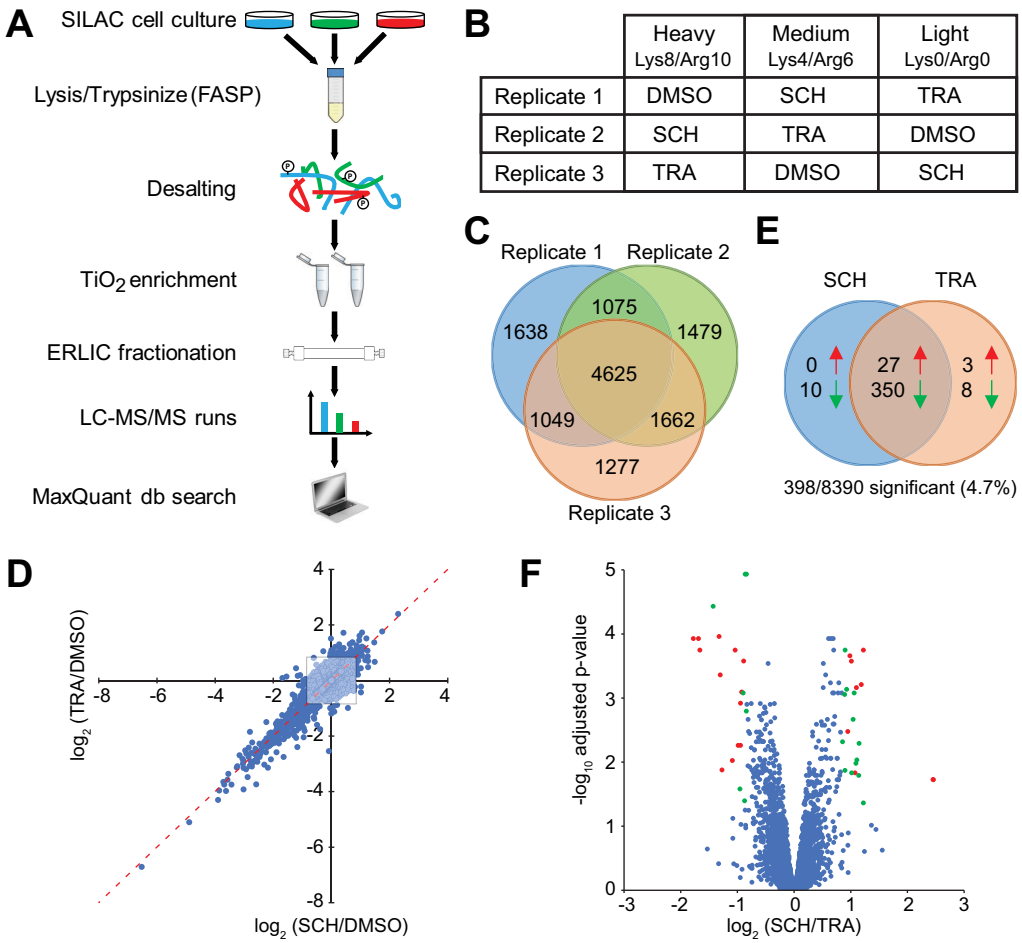

FIG. 1. **Phosphoproteomics responses to trametinib *versus* SCH772984.** *A*, Experimental workflow, involving SILAC labeling of cultured WM239A cells, FASP proteolysis, phosphopeptide enrichment and fractionation, and LC-MS/MS. *B*, Scheme of isotope labeling and mixing in three biological replicates, treating cells for 2 h with DMSO, 10 μM SCH772984 (SCH), or 10 μM trametinib (TRA). *C*, Overlap between biological replicate experiments identified 12,805 quantifiable Class I phosphosites, of which 8390 were quantifiable in two or more replicates. *D*, Log_2-transformed ratios showing responses to SCH or TRA compared with DMSO control, among 8390 phosphosites that could be quantified in at least two biological replicates. Opaque region shows the significance cutoff of $|\log_2(\text{combined ratio})| \geq 0.84$. *E*, Numbers of phosphosites that can be quantified with both TRA and SCH and also changed significantly in response to either inhibitor, based on $|\log_2(\text{combined ratio})| \geq 0.84$, and adjusted p value < 0.05. *F*, Volcano plot showing confidence (adjusted p value) *versus* $\log_2$-transformed SCH:TRA ratio, among the 8,390 phosphosites. Phosphosites that passed both the significance threshold of $|\log_2(\text{combined ratio})| \geq 0.84$ and confidence threshold of $p < 0.05$ are colored red or green. Of these, red indicates sites that responded significantly to only one inhibitor, as shown in panel *E* (13 sites decreased only with SCH or increased only with TRA; 8 sites decreased only with TRA or increased only with SCH).

RESULTS

Phosphoproteomics Responses to Trametinib and SCH772984—We used phosphoproteomics to compare molecular responses to the MKK1/2 inhibitor, trametinib, and the ERK1/2 inhibitor, SCH772984, in WM239A human metastatic melanoma cells. To quantify changes in phosphorylation, SILAC labeled cells (light, medium, or heavy) were treated with DMSO, 10 μM trametinib, or 10 μM SCH772984 for 2 h followed by cell lysis, trypsinization, and phosphopeptide enrichment with TiO_2 resin, and fractionation by ERLIC chromatography (5, 16, 17) (Fig. 1*A*). Experiments were conducted in biological triplicates and the isotopic labels for each condition were varied between replicates (Fig. 1*B*). In total, SILAC ratios were quantified for 12,805 class I phosphosites (18) on 3819 proteins (supplemental Table S1). Of these, 8390 could be quantified in two or more replicate experiments (Fig. 1*C*, supplemental Table S1). ERLIC chromatography into 24 fractions increased phosphopeptide identifications, with >95% of phosphopeptides showing single phosphorylation sites (supplemental Fig. S1).

A threshold of 1.8-fold ($\log_2 \pm 0.84$) was used to identify phosphosites with significant changes in abundance after inhibitor treatment, based on control experiments previously reported by our lab using the same cell line (5). After filtering with this threshold, 553 class I phosphosites were found to be altered significantly by one or both inhibitors in multiple replicates

(Fig. 1*D*). As an additional filter for significant changes, an empirical Bayesian analysis using the Limma statistical package was employed to calculate adjusted *p* values for each phosphosite (11). We focused our remaining analysis on the 398 phosphosites that exhibited average fold changes of 1.8-fold or more, and an adjusted *p* value of < 0.05 (Fig. 1*E*, supplemental Table S1).

Non-TiO_2-enriched proteolytic digests were analyzed by 2D LC-MS/MS to assess changes at the protein level. Few proteins showed significant changes in abundance after 2 h of inhibitor treatment (supplemental Table S2). Only one, FOSL1, showed a significant change in protein abundance that could account for its phosphorylation response to trametinib or SCH772984 (S191, supplemental Table S3). This was consistent with destabilization and proteasomal degradation of FOSL1 in response to ERK1/2 inhibition, described previously (19).

Of the 388 phosphosites significantly regulated by trametinib, 377 (95%) significantly responded in the same direction with SCH772984 (Fig. 1*D*, 1*E*). As expected, the regulatory phosphosites on ERK1 and ERK2, which are the primary targets of MKK1/2, were among those most strongly inhibited by trametinib (supplemental Fig. S2). The same sites were also inhibited by SCH772984, reflecting the ability of this ERK inhibitor to induce disorder in the activation loop of ERK1/2 and interfere with its phosphorylation by MKK1/2 (20) (supplemental Fig. S2).

The results showed that the majority of phosphosites responsive to an MKK1/2 inhibitor paralleled those responsive to an ERK1/2 inhibitor, consistent with their regulation downstream of ERK. Similar behavior was observed in a previous phosphoproteomics study, where phosphosites responsive to the BRAF inhibitor, vemurafenib, paralleled those responsive to the MKK1/2 inhibitor, selumetinib (5). Taken together, the results from the two experiments reveal linearity in signaling through the MKK-ERK pathway, downstream of oncogenic BRAF (5).

A volcano plot (Fig. 1*F*) shows the adjusted *p* values for all phosphosites shown in Fig. 1*D*, highlighting those showing the greatest difference between inhibitors, based on $\log_2$ (SCH772984/trametinib) ratios. Of all significant phosphosites, only 21 were significantly altered only by trametinib or only by SCH772984 (Fig. 1*E*, 1*F*, supplemental Table S1). Of these, 11 phosphosites responded to trametinib but not SCH772984, of which 8 decreased and 3 increased with inhibitor, whereas 10 phosphosites responded to SCH772984 but not trametinib, each of which was inhibited by drug (Fig. 1*E*, supplemental Table S1). The strongest effects unique to trametinib occurred at the regulatory phosphorylation sites on MKK1 (MAP2K1) and MKK2 (MAP2K2), reflecting interference of the drug-bound MKK1/2 to phosphorylation by BRAF (21) (supplemental Fig. S2).

Trametinib Inhibits p38α MAPK Phosphorylation at Regulatory Sites—Interestingly, two phosphorylation sites that responded only to trametinib were those that regulate the activity of p38α MAPK (MAPK14) (supplemental Table S1). Phosphorylation of p38α MAPK at both Thr180 and Tyr182, respectively, decreased by 2.2- and 1.9-fold with trametinib, but remained almost unchanged with SCH772984 (Fig. 2*A*, supplemental Fig. S2). These were the only phosphosites on a protein kinase other than MKK1/2 that responded to only one and not both inhibitors (supplemental Table S1). Of the four isoforms of p38 MAPK (α, β, γ, δ), p38α is the best characterized and the most consistently expressed across cell types (22, 23). RNA-seq analysis showed that this isoform was the most highly expressed in WM239A cells (data not shown). It was also the only isoform of p38 observed in our total protein data set (supplemental Table S2). The results suggested that an inhibitor of MKK1/2-ERK1/2 signaling might also inhibit the stress-dependent MAPK pathway.

To determine if other MKK1/2 inhibitors besides trametinib also blocked phosphorylation of p38α MAPK, we examined the results of a previous data set measuring phosphoproteomic responses to selumetinib and the BRAF inhibitor, vemurafenib (5). Neither Thr180 nor Tyr182 in p38α MAPK responded significantly to selumetinib or vemurafenib (Fig. 2*A*). Thus, the ability of trametinib to block p38α MAPK phosphor ylation appears to be an off-target effect, unique to this drug.

Importantly, phosphorylation of Ser796 on the epidermal growth factor receptor pathway substrate 15 (EPS15) was also inhibited by trametinib but not selumetinib (supplemental Table S4). In HeLa cells, this phosphosite was shown to decrease in response to p38 MAPK inhibitor (SB203580), but not MKK1/2 inhibitor (U0126) nor JNK inhibitor (SP600125) (24). Thus, trametinib selectively inhibits the phosphorylation of a specific substrate of p38 MAPK as well. This provides evidence that the off-target effect of trametinib inhibits a downstream target of the p38α MAPK pathway, not associated with BRAF-MKK-ERK signaling.

To confirm direct inhibition of p38α MAPK phosphorylation by trametinib, we conducted a series of biochemical assays. Anti-phospho-p38 antibodies do not distinguish between different isoforms of p38 MAPK, and fail to detect basal levels of p38 phosphorylation in WM239A cells. Therefore, an isoform-specific antibody was used to immunoprecipitate and enrich p38α MAPK, followed by Western blotting with anti-phospho-p38 antibody. Treating cells with trametinib for 2 h led to significant inhibition of p38α phosphorylation compared with cells treated with DMSO or SCH772984 (Fig. 2*B*). The magnitude of inhibition by trametinib reached 50%, comparable to the magnitude observed by phosphoproteomics (Fig. 2*A*).

We next sought to determine how trametinib might affect the activation of p38α MAPK by stress responses, such as hyperosmotic stress. Cells were pretreated with trametinib, selumetinib, or SCH772984 for 2 h, before raising the osmolality of media from 300 mOsm to 500 mOsm by addition of a solution of NaCl + KCl (12.5:1) (25, 26). Hyperosmotic stress

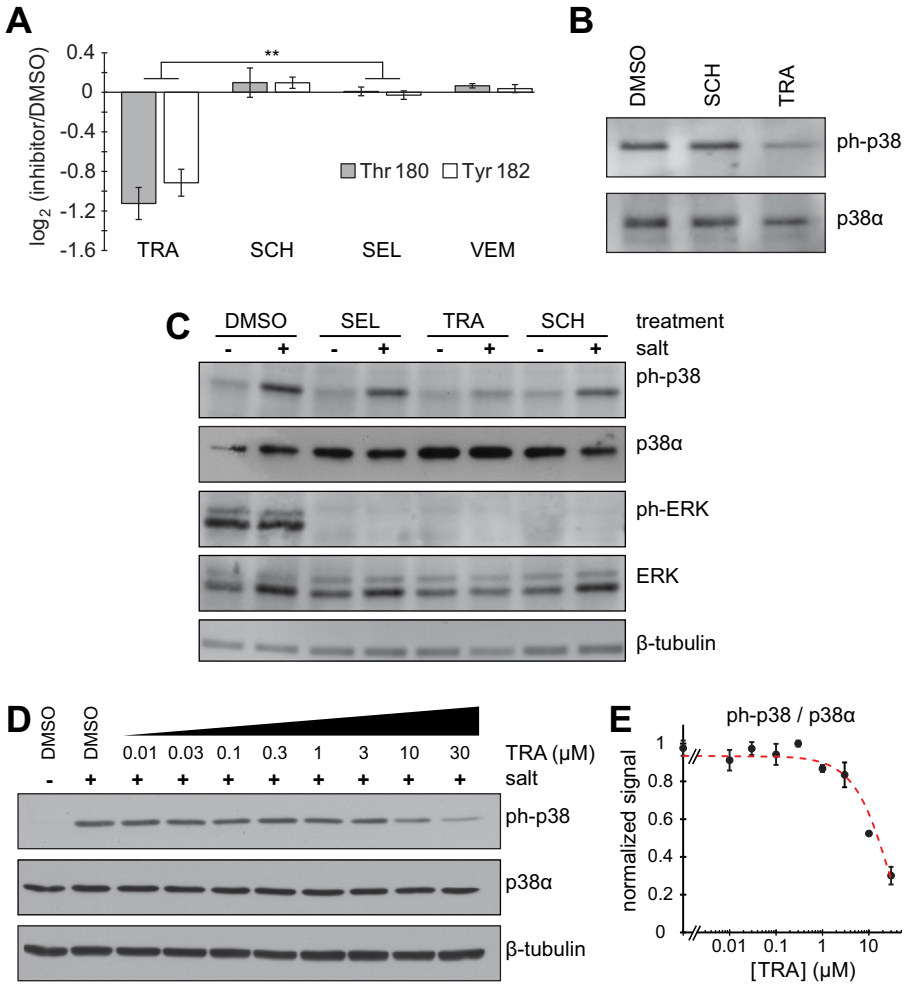

FIG. 2. **Trametinib inhibits p38α MAPK phosphorylation.** *A*, Log_2(combined ratio of inhibitor:DMSO), quantified for the Thr180 and Tyr182 activating phosphorylation sites on p38α MAPK. Values show log_2(ratio) observed with the MKK1/2 inhibitors, trametinib (TRA) and selumetinib (SEL), the ERK1/2 inhibitor, SCH772984 (SCH), and BRAF inhibitor vemurafenib (VEM) (each treated for 2 h with 10 μM inhibitor). Data for SEL and VEM are from Stuart *et al.* (5). Asterisks indicate significance of $p < 0.004$. *B*, Immunoprecipitation of p38α MAPK from lysates of cells treated for 2 h with DMSO, 10 μM TRA, or 10 μM SCH, followed by Western blotting with anti-phospho-p38 (Thr180/Tyr182) and anti-p38α MAPK antibodies. *C*, Stimulation of p38 phosphorylation by hyperosmotic stress. Cells were pre-treated for 30 min with DMSO or 10 μM SEL, TRA or SCH, then stimulated without or with NaCl + KCl for 2 h to raise the media osmolality from 300 mOsm to 500 mOsm. Lysates were examined by Western blotting with anti-phospho-p38 (Thr180/Tyr182), anti-p38α MAPK, anti-phospho-ERK1/2 (Thr202/Tyr204 and Thr185/Tyr187), and anti-ERK1/2 antibodies, as well as anti-β-tubulin as a loading control. *D*, Dose response of TRA effects on phospho-p38 MAPK. Cells were pretreated for 30 min with DMSO or TRA at varying concentrations, then stimulated without or with NaCl + KCl for 2 h. Western blots show reactivity with anti-phospho-p38 (Thr180/Tyr182), anti-p38α MAPK and anti-beta-tubulin antibodies. *E*, Quantification of anti-phospho-p38 immunoreactivity normalized to p38α MAPK signal. Data are from Western blots of biological triplicate experiments, quantified using ImageJ.

resulted in elevated phosphorylation of p38α MAPK, which was inhibited by trametinib, but not selumetinib or SCH772984 (Fig. 2*C*). We also established a dose response for inhibition of p38α phosphorylation by varying the concentration of trametinib in the 2 h preincubation before salt addition, which yielded an estimated IC_{50} ~10 μM (Fig. 2*D*, 2*E*). Thus, the off-target effect of trametinib on p38α MAPK phosphorylation occurs at concentrations used in the literature, although higher than those achieved clinically (27, 28).

We next asked how trametinib inhibits p38α MAPK phosphorylation. The specificity of trametinib for MKK1/2 suggested that it might also directly target MKK6, which is known to phosphorylate and activate p38α during stress responses, including hyperosmotic treatment (23). Previous kinase activity screens using *in vitro* ELISA or mobility shift assays have characterized trametinib as a strong inhibitor of the target kinase, MKK1/2, but a weak inhibitor (and in some cases a weak activator) of MKK6 (27, 29). On the other hand, MKK1 and MKK6 share sequence identity in most of the residues identified in crystal structures to interact with non-ATP competitive inhibitors of MKK1, such as trametinib (30, 31) (supplemental Fig. S3). Therefore, we examined MKK6 inhibition by trametinib using *in vitro* kinase assays. Flag-MKK6 was expressed as wild-type (WT), constitutively active (S207E/

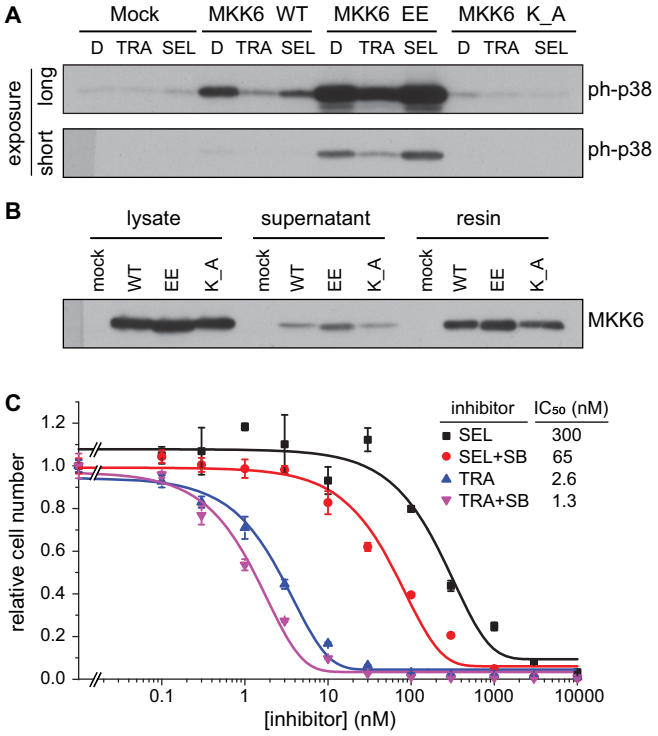

FIG. 3. **Trametinib inhibits MKK6 *in vitro*, and in cells is nonsynergistic with a p38 MAPK inhibitor.** *A*, Flag-MKK6 was expressed in WM239A cells, in wild type (WT), constitutively active (EE), or catalytically inactive (K_A) mutant forms, then immunoprecipitated with anti-Flag antibody, and incubated for 15 min with DMSO (D), 10 μM trametinib (TRA) or 10 μM selumetinib (SEL). *In vitro* kinase activity was measured by phosphorylating recombinant unphosphorylated p38α MAPK for 15 min at 30 °C and quantifying phosphorylation by Western blotting with anti-phospho-p38 antibody (Thr180/Tyr182). *B*, Loading controls showing reactivity with Flag-MKK6, in the *in vitro* kinase assays of panel *A*. *C*, Cell viability assays of WM239A cells treated with varying concentrations of TRA or SEL, with or without the p38 inhibitor, SB203580 (10 μM). SB203580 augments the inhibition of cell viability with SEL, but has less effect on cell viability with TRA.

T211E, "EE"), or catalytically inactive (K82A, "K_A") forms in WM239A cells, and then immunoprecipitated with anti-Flag antibody. Immunoprecipitated MKK6 was then preincubated with DMSO, trametinib, or selumetinib, and kinase reactions were initiated by addition of unphosphorylated p38α substrate and Mg-ATP (Fig. 3*A*, 3*B*). As expected, the Flag-MKK6-EE mutant exhibited much higher activity toward p38α MAPK than Flag-MKK6-WT (Fig. 3*A*) (14). Trametinib inhibited p38α MAPK phosphorylation by MKK6-WT and MKK6-EE to similar degree (Fig. 3*A*, 3*B*). In contrast, selumetinib had minimal effect on MKK6 activity. Therefore, MKK6 is a direct target of trametinib but not selumetinib, leading to decreased p38α MAPK phosphorylation *in vitro*.

Finally, we asked if the ability of trametinib to inhibit p38α MAPK might contribute to the effect of trametinib on the viability of WM239A cells. We reasoned that if the off-target effect of trametinib on p38α MAPK influenced cell viability, addition of a p38α MAPK inhibitor might augment the effects of other MKK1/2 inhibitors more than it would with trametinib. To address this, we added the p38α/β MAPK inhibitor, SB203580, to WM239A cells treated with trametinib or selumetinib at varying concentrations, and measured cell numbers after 72 h. Added alone at 10 μM, SB203580 had no inhibitory effect on cell viability (data not shown). However, in combination, SB203580 reduced the IC_{50} for selumetinib by nearly 5-fold, from 300 nM in the absence of SB203580 to 65 nM in its presence (Fig. 3*C*). In contrast, SB203580 had a smaller effect on the IC_{50} for trametinib, decreasing it by only 2-fold (Fig. 3*C*). The findings are consistent with a model in which the p38α inhibitor augments the effect of MKK1/2 inhibition by selumetinib, but has less effect on trametinib because of the latter's off-target inhibition of p38α MAPK. The results suggest that the off-target effect of trametinib on MKK6 and p38α MAPK may contribute to its ability to interfere with cell proliferation at high concentrations.

Comparison of ERK1/2 Inhibitors SCH772984 and GDC0994 — Having identified an intriguing off-target effect specific to trametinib, we investigated the potential for differential responses between two high affinity inhibitors of ERK1/2, SCH772984 (32) and GDC0994 (8). To do this, we conducted another triple-labeled phosphoproteomics experiment, comparing WM239A cells treated with DMSO, 10 μM SCH772984 and 10 μM GDC0994. Biological triplicate experiments identified 7074 class I phosphorylation sites on 2876 proteins, including 5382 phosphosites quantified in at least two replicates (Fig. 4*A*, supplemental Fig. S4, supplemental Table S5).

Of the 5382 phosphosites, 325 were significantly responsive to at least one ERK1/2 inhibitor, of which 288 (88%) were regulated in the same direction with both SCH772984 and GDC0994 (Fig. 4*B*). Six phosphosites decreased uniquely in response to SCH772984 (Fig. 4*B*, 4*C*, supplemental Table S5). Of these, three corresponded to the regulatory phosphorylation sites within the activation loop of ERK1 or ERK2 (Tyr204 in hERK1; Tyr187/Thr190 in hERK2). This reflects the ability of SCH772984, but not GDC0994, to inhibit ERK1/2 phosphorylation by MKK1/2 (supplemental Fig. S2), through distortion of the ERK activation segment (7). Thus, only three targets unique to SCH772984 could not be explained by its property of ERK binding. In contrast, 31 phosphosites were unique to GDC0994 (Fig. 4*B*). Therefore, GDC0994 appears to be a more promiscuous inhibitor, based on the larger number of phosphosites that respond to treatment with GDC0994, but not with SCH772984.

*Combined Analyses of Four Inhibitors of MKK1/2 or ERK1/2—*To evaluate the phosphoproteomic responses to two MKK1/2 inhibitors, we compared trametinib:DMSO ratios (Fig. 1) against selumetinib:DMSO ratios from the previous data set (5). In total, 6386 phosphosites were reproducibly quantified in at least two replicates in both experiments (Fig. 4*D*). Of these, 249 were significantly inhibited in response to both trametinib and selumetinib (Fig. 4*E*). Of phosphosites significantly inhibited by either treatment, only 10 were inhibited by tra-

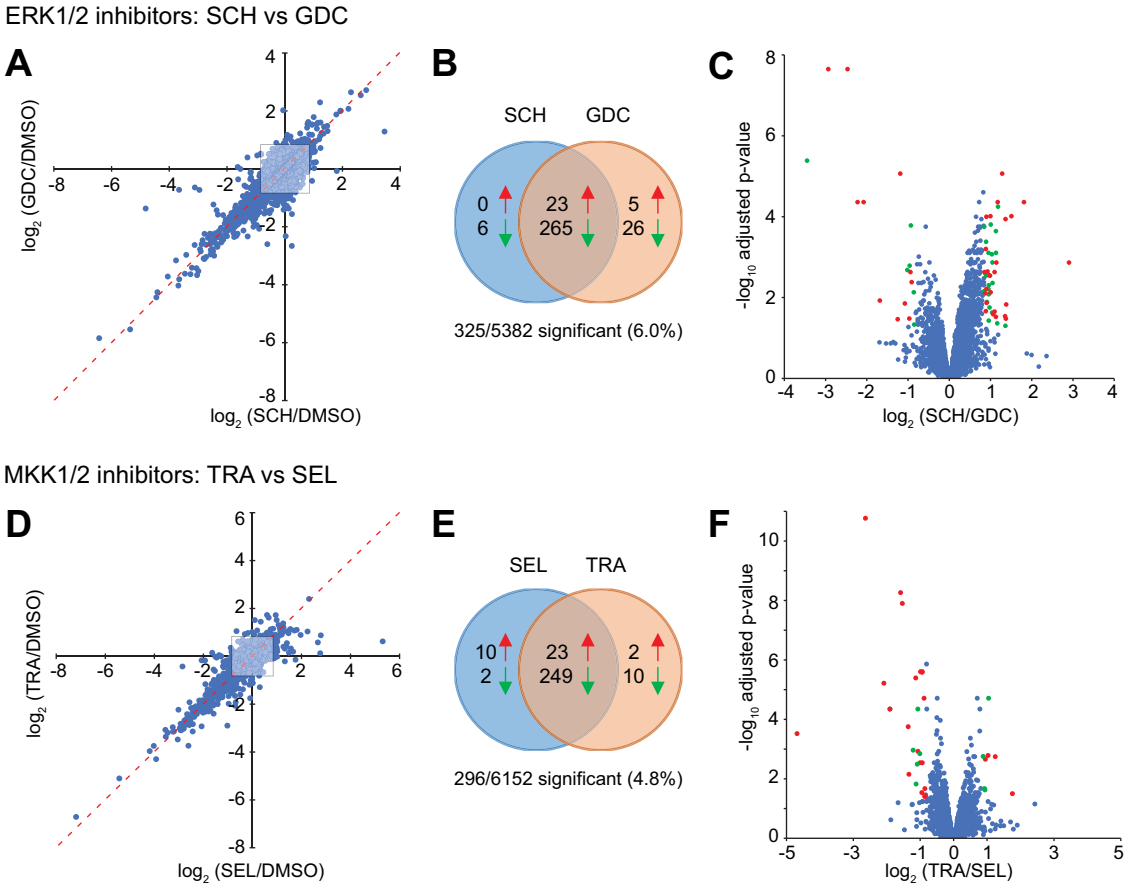

FIG. 4. **Phosphoproteomics comparison of ERK1/2 inhibitors (SCH772984 *versus* GDC0994) and MKK1/2 (trametinib *versus* selumetinib) inhibitors.** *A*, Log_2-transformed ratios showing responses to SCH772984 (SCH) or GDC0994 (GDC) compared with DMSO control, in 5382 phosphosites observed reproducibly in at least two replicates of SILAC labeled cells (see further characterization in supplmental Fig. S4). Opaque region shows significance cutoff of $|\log_2(\text{combined ratio})| \geq 0.84$. *B*, Numbers of significantly altered phosphosites that were quantified with both SCH and GDC, and also changed significantly in response to either inhibitor, based on $|\log_2(\text{combined ratio})| \geq 0.84$, and adjusted p value < 0.05. *C*, Volcano plot showing confidence (adjusted p value) *versus* $\log_2$ transformed ratio of SCH:GDC for the 5382 phosphosites. Phosphosites that passed both the significance threshold of $|\log_2(\text{combined ratio})| \geq 0.84$ and confidence threshold of $p < 0.05$ are colored red or green. Of these, red indicates sites that responded significantly to only one inhibitor, as shown in panel *B* (11 sites decreased only with SCH or increased only with GDC; 26 sites decreased only with GDC). *D*, Log_2-transformed ratios showing responses to trametinib (TRA) or selumetinib (SEL) compared with DMSO control, in 6386 phosphosites that could be quantified in at least two biological replicates. Data for TRA are from this study (see Fig. 1), and data for SEL are from a previous study in the same cell line (5). Opaque region shows significance cutoff of $|\log_2(\text{combined ratio})| \geq 0.84$. *E*, Numbers of phosphosites that can be quantified with both TRA and SEL and also changed significantly in response to either inhibitor, based on $|\log_2(\text{combined ratio})| \geq 0.84$, and adjusted p value < 0.05. *F*, Volcano plot showing confidence (adjusted p value) *versus* $\log_2$-transformed ratio of TRA:SEL for the 6386 phosphosites. Phosphosites that passed both the significance threshold of $|\log_2(\text{combined ratio})| \geq 0.84$ and confidence threshold of $p < 0.05$ are colored red or green. Of these, red indicates sites that responded significantly to only one inhibitor, as shown in panel *E* (20 sites decreased only with TRA or increased only with SEL; 4 sites decreased only with SEL or increased only with TRA).

metinib but not selumetinib, whereas 2 were inhibited by selumetinib but not trametinib (Fig. 4*E*, 4*F*, supplemental Table S4). Thus, more than 95% of responsive phosphosites were inhibited by both trametinib and selumetinib.

The information from phosphoproteomics data on the two MKK1/2 inhibitors (trametinib, selumetinib) were then combined with the two ERK1/2 inhibitors (SCH772984, GDC0994) to further analyze inhibitor and pathway specificity. Combining all experiments, 3658 phosphosites (3743 phosphopeptides) could be reproducibly quantified across all four inhibitor treatments (supplemental Table S6). The overlap between phosphosites responding significantly to each compound is summarized in Fig. 5*A*.

In total, 161 phosphosites were significantly altered in response to all four inhibitors, each with inhibitor/control ratios exceeding the threshold of $|\log_2(\text{combined ratio})| > 0.84$. Phosphosites that were inhibited by all four compounds likely represent *bona fide* downstream targets of the BRAF-MKK1/2-ERK1/2 pathway. They included 152 phosphosites that decreased and 9 that increased in response to each treatment. We examined this set for phosphosites that could be direct substrates of ERK1/2. Among the 152 phosphorylation sites

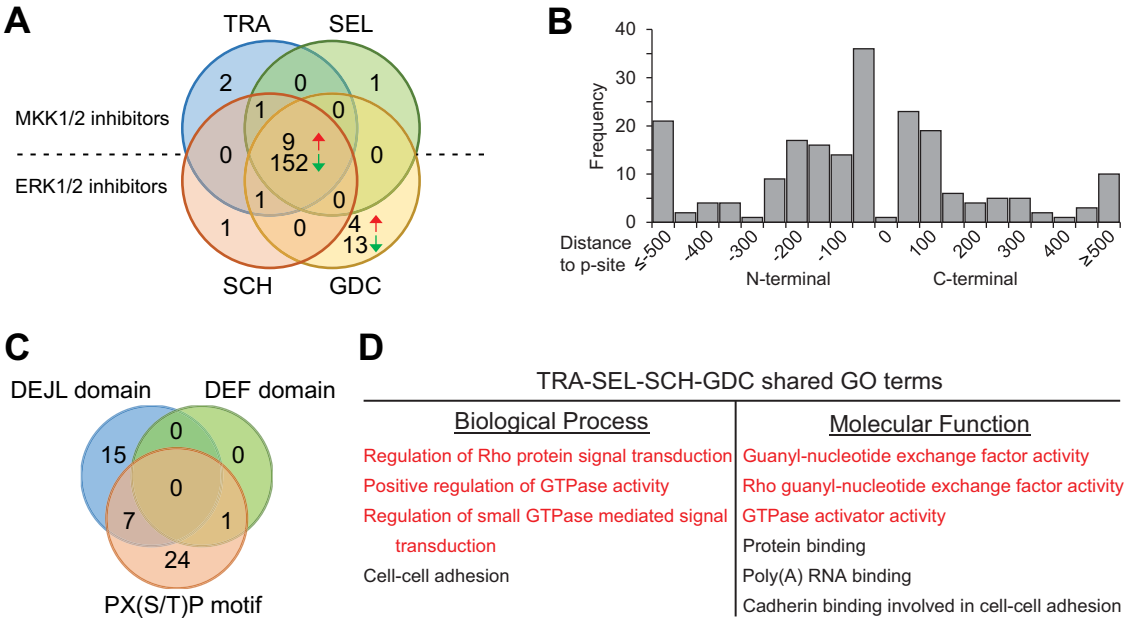

FIG. 5. **Overlap between phosphosites altered significantly in response to all four MKK1/2 or ERK1/2 inhibitors.** *A*, Venn diagram summarizing phosphosites responsive to selumetinib (SEL), trametinib (TRA), SCH772984 (SCH) or GDC0994 (GDC), based on $|\log_2(\text{combined ratio})| \geq 0.84$, each from at least 2 replicate measurements. Results were compiled from three SILAC phosphoproteomics data sets, including DMSO-TRA-SCH and DMSO-SCH-GDC (this study), and DMSO-SEL-VEM (vemurafenib) (5). Phosphosites from SCH treatment in the two data sets of this study were combined. In total, 3658 phosphosites could be compared quantitatively for each inhibitor, of which 3289 showed no significant change in response to any inhibitor. One hundred sixty-one were found regulated by all inhibitors, and are interpreted as *bona fide* MKK1/2-ERK1/2 pathway targets. *B*, Histogram summarizing DEJL motifs identified by Zeke *et al.* (47), showing their closest distance (measured from the center of the motif) to 203 known phosphorylation sites in substrates of ERK1/2 documented by Yoon & Seger (34) or Phosphosite (37). Of the 203 sites, 126 (62%) fell within −200/+100 residues of the phosphorylation site recognized by ERK1/2. We applied this position window as a filter for identifying DEJL motifs in ERK1/2 substrates. *C*, Venn diagram showing characteristics of 47 potential phosphorylation sites for ERK1/2, filtered based on the presence of ERK substrate identifiers, including Pro at position P-2 and/or DEF or DEJL motifs. *D*, GO terms identified by the DAVID bioinformatics tool, examining genes corresponding to significantly regulated phosphosites in response to TRA (342 unique genes), SEL (527 unique genes), SCH (332 unique genes), and GDC (313 unique genes). GO terms identified with *p* value and FDR < 0.05. Terms in red are associated with processes involving GTPase signaling.

that decreased in response to all four inhibitors, 103 harbored the canonical Ser/Thr-Pro sequence for ERK1/2 substrate recognition. Of these, 21 (20%) matched a list of 783 validated target sites for ERK1/2 (supplemental Table S7). The validated sites were from a database by Unal *et al.* (33) who compiled information from a literature review by Yoon and Seger (106 sites) (34), proteins phosphorylated *in vitro* by ERK1 (87 sites) (35), proteins phosphorylated *in vitro* by an analog-sensitive mutant of ERK2 (92 sites) (36), phosphosites targeted by ERK in the PhosphoSitePlus database (693 sites) (37), and five validated ERK phosphosites mapped by other studies (38–40).

The remaining 82 phosphosites that decreased in response to inhibitor, but are not a part of this database, are candidates for being novel targets of ERK1/2. We inspected their proximity to three identifiers often found in MAP kinase substrates, including Pro present at position P-2 in the consensus sequence Pro-Xxx-pSer/pThr-Pro (41) and two docking motifs. One docking motif, named "DEF" (*aka* FRS), binds a pocket near the activation segment of ERK1/2 and typically contains the consensus hydrophobic sequence Phe/Tyr-Xxx-Phe/Tyr located 6–20 residues C-terminal to the phosphorylation site (42, 43). A second motif, named "DEJL" (*aka* D-domain or DRS), binds a pocket distal to the catalytic cleft in ERK1/2, and often contains the consensus sequence $(\text{Arg/Lys})_{2-3}$-$(\text{Xxx})_{2-6}$-Φ_A-Xxx-Φ_B, where Φ_A and Φ_B are hydrophobic residues (44). DEJL motifs are more commonly observed, but can be harder to identify because they do not share exact consensus sequences and can vary in their distances from the phosphorylation site (43, 45, 46). A recent study mapped candidate DEJL docking motifs across the human proteome, by combining analyses of sequence and structural compatibility/surface topography for protein-protein interactions (47). We calculated the distances between these candidate DEJL motifs and their nearest known ERK-targeted sites within the substrates compiled by Yoon and Seger (34) and PhosphoSitePlus (37). Of 203 DEJL motifs that could be mapped to proteins containing ERK-phosphorylated residues, the majority were positioned within 200 residues N-terminally, and 100 residues C-terminally from the phosphorylation site (Fig. 5*B*). We therefore examined candidate ERK1/2 sites in our data set for DEJL motifs within this window, using the

TABLE I
Phosphorylation sites decreased in response to all MKK1/2 or ERK1/2 inhibitors, with ERK target identifiers

Uniprot ID	Gene name	Protein name	Position	Pro-2	DEJL[a]	DEF[b]	TRA/DMSO[c]	SEL/DMSO[c]	SCH/DMSO[c]	GDC/DMSO[c]
Q9P2F8	SIPA1L2	Signal-induced proliferation-associated 1-like 2	S1461	YES		FxF	−2.21	−2.25	−2.31	−2.20
Q9Y2D5	AKAP2	A-kinase anchor protein 2	S152	YES	−40		−1.25	−1.33	−1.16	−1.24
Q53ET0	CRTC2	CREB-regulated transcription coactivator 2	S433	YES	−186		−1.70	−1.43	−1.51	−1.82
Q6Y7W6	GIGYF2	PERQ amino acid-rich with GYF containing protein 2	S593	YES	−70		−1.97	−2.15	−1.95	−2.01
Q9Y4H2	IRS2	Insulin receptor substrate 2	S1203	YES	−13		−1.71	−1.44	−1.46	−1.38
Q8NFH5	NUP35	Nucleoporin NUP53	T48	YES	+65		−1.31	−1.40	−1.50	−1.41
O43379	WDR62	WD repeat-containing protein 62	S1348	YES	−57		−1.01	−0.98	−1.23[d]	−1.25
O43149	ZZEF1	Zinc finger ZZ-type and EF-hand containing protein 1	S1518	YES	−93		−1.80	−1.67	−1.61	−1.22
Q9H3P7	ACBD3	Golgi resident protein GCP60	S43	YES			−1.30	−1.49	−1.27	−1.56
O43572	AKAP10	A-kinase anchor protein 10, mitochondrial	S187	YES			−0.98	−0.91	−1.16	−1.01
Q9Y6D6	ARFGEF1	Brefeldin A-inhibited guanine nucleotide-exchange 1	S1555	YES			−2.11	−1.98	−1.64	−1.57
Q92888	ARHGEF1	Rho guanine nucleotide exchange factor 1	S863	YES			−1.46	−1.12	−1.35	−0.99
Q96PE2	ARHGEF17	Rho guanine nucleotide exchange factor 17	S527	YES			−1.07	−1.55	−0.88[d]	−1.05
Q96LT7	C9orf72	Protein C9orf72	S9	YES			−2.65	−2.73	−2.46	−2.34
Q5T5Y3	CAMSAP1	Calmodulin-regulated spectrin-associated protein 1	S1080	YES			−2.28	−2.07	−2.06	−1.76
Q5T5Y3	CAMSAP1	Calmodulin-regulated spectrin-associated protein 1	T1144	YES			−2.13	−2.00	−1.79	−2.15
Q9Y4F5	CEP170B	Centrosomal protein of 170 kDa protein B	S1548	YES			−1.53	−1.32	−1.13	−1.16
O43310	CTIF	CBP80/20-dependent translation initiation factor	S299	YES			−2.22	−2.27	−2.04	−1.88
Q9Y6G9	DYNC1LI1	Cytoplasmic dynein 1 light intermediate chain 1	T513	YES			−1.39	−0.95	−1.05	−0.99
Q63ZY3	KANK2	KN motif and ankyrin repeat containing protein 2	S19	YES			−0.84	−0.99	−0.84	−1.11
P78559	MAP1A	Microtubule-associated protein 1A	T504	YES			−2.82	−2.93	−3.06	−2.26
Q7Z434	MAVS	Mitochondrial antiviral-signaling protein	S222	YES			−1.67	−1.64	−1.53	−1.68
Q9HCH0	NCKAP5L	Nck-associated protein 5-like	S763	YES			−1.12	−1.15	−1.03	−1.58
Q86WR7	PROSER2	Proline and serine-rich protein 2	S215	YES			−2.00	−1.42	−1.88	−1.43
Q70E73	RAPH1	Ras-associated and pleckstrin homology containing 1	S1154	YES			−1.06	−0.93	−0.87	−1.11
Q9NZJ4	SACS	Sacsin	S4264	YES			−2.26	−1.71	−1.81	−1.79
Q07157	TJP1	Tight junction protein ZO-1	S1617	YES			−1.32	−1.53	−1.35	−1.43
Q86T03	TMEM55B	Type 1 PtdIns-4,5-P2 4-Ptase	S162	YES			−1.38	−1.38	−1.39	−1.49
Q9NS69	TOMM22	Mitochondrial import receptor subunit TOM22 homolog	S15	YES			−1.34	−1.29	−1.13	−1.41
Q96LD4	TRIM47	Tripartite motif-containing protein 47	S588	YES			−3.48	−3.05	−2.88	−2.62
P40222	TXLNA	Alpha-taxilin	S515	YES			−1.23	−1.35	−1.23	−0.98
Q9C0C9	UBE2O	E2/E3 hybrid ubiquitin-protein ligase UBE2O	S839	YES			−1.77	−1.80	−1.54	−1.75
Q09666	AHNAK	Neuroblast differentiation-associated protein AHNAK	S3426		−9		−2.53	−2.38	−2.41	−2.77
Q09666	AHNAK	Neuroblast differentiation-associated protein AHNAK	S2397		+6		−2.42	−2.66	−2.84	−3.04
Q09666	AHNAK	Neuroblast differentiation-associated protein AHNAK	S511		+75		−1.14	−1.30	−1.39	−1.08
Q9UKA4	AKAP11	A-kinase anchor protein 11	S448		−113		−1.29	−1.34	−1.34	−1.76
Q9HCE9	ANO8	Anoctamin-8	S641		−141		−1.04	−1.41	−1.40	−1.12
Q9Y6I3	EPN1	Epsin-1	S435		−200		−2.18	−2.08	−1.97	−1.89
Q4G0A6	FAM188B	Protein FAM188B	S392		+50		−1.87	−1.63	−1.76	−1.82
O14686	*KMT*2D	Histone-lysine N-methyltransferase 2D	S2274		−172		−1.51	−1.40	−1.29	−1.49
Q8IY33	MICALL2	MICAL-like protein 2	S726		−57		−3.03	−2.81	−2.31	−2.44
Q6WCQ1	MPRIP	Myosin phosphatase Rho-interacting protein	S619		−20		−0.94	−0.98	−1.06	−0.95
Q5SYE7	NHSL1	NHS-like protein 1	S1292		−88		−1.06	−0.86	−0.85	−1.01
O75665	OFD1	Oral-facial-digital syndrome 1 protein	S774		−104		−1.00	−1.00	−1.03[d]	−1.00
Q8IY67	RAVER1	Ribonucleoprotein PTB-binding 1	T463		−25		−1.22	−1.25	−1.11	−1.44
Q8NC51	SERBP1	Plasminogen activator inhibitor 1 RNA-binding protein	S234		+96		−1.89	−1.74	−2.08	−1.61
Q9Y3Q8	TSC22D4	TSC22 domain family protein 4	S279		−40		−3.09	−2.91	−2.74	−2.51

[a] Domain identified within positions P-200 to P + 100 from the phosphosite, indicating residue number for the closest distance in parentheses.

[b] Domain identified within positions P + 6 to P + 20 from the phosphosite.

[c] Empirical Bayes-generated $\log_2$(combined ratio) ($n \geq 2$) of SILAC replicates for each experiment.

[d] Significant response from measurements in DMSO-SCH772984-GDC0994 experiment. All other SCH:DMSO measurements are from the DMSO-trametinib-SCH772984 experiment.

published study (47) as well as ScanSite3 (48) to identify DEJL sequences.

Among the 82 candidates for direct targets of ERK1/2, 47 contained at least one additional identifier of ERK1/2 substrates. Thirty-two sites were adjacent to Pro at the P-2 position, 22 showed DEJL sequences located between positions P-200 to P + 100, and 1 showed a DEF sequence located between positions P + 6 to P + 20 (Fig. 5*C*, Table I). A significant number were phosphosites on proteins that regulate small GTPase signaling. They included signal-induced proliferation-associated 1-like protein 2 (SIPA1L2), a Rap GTPase activating protein (RapGAP) (49), with phosphoryla-

tion site Ser1461 adjacent to Pro-2 as well as DEF motif identifiers, phosphosite Ser619 on myosin phosphatase Rho-interacting protein (MPRIP) adjacent to a DEJL motif, and three sites on Rho guanine nucleotide exchange factors (Ser863 on ARHGEF1, Ser1555 on ARFGEF1, and Ser527 on ARFGEF17) which were adjacent to Pro at position P-2 or DEJL motifs. In addition, Ser726 on the Rab effector, MICALL2, which functions in F-actin depolymerization, and Ser9 on the Rab interactor, C9orf72, which functions in endosomal trafficking, were nearby Pro-2 or DEJL motifs. Proteins involved in small GTPase signaling were also highly represented when all genes containing phosphosites significantly regulated by trametinib, selumetinib, SCH772984, or GDC0994 were combined for examination by gene ontology (GO) analysis using the bioinformatics resource, DAVID (50) (Fig. 5*D*). Together, these candidates suggest potential new cross-regulatory mechanisms for control of small GTPase signaling by ERK1/2, downstream of oncogenic BRAF.

Other interesting candidates had the potential to regulate protein activity, stability or gene expression, including Ser162 on the lipid phosphatase, TMEM55B, Ser2274 on the histone H3K4me methyltransferase, KMT2D, and Ser279 on the transcription repressor, TSC22D4. TSC22D4 promotes the bypass of oncogene-induced senescence mediated by $BRAF^{V600E}$ when overexpressed in fibroblasts (51), suggesting its potential control by ERK phosphorylation in melanoma.

We next examined cases where phosphosites were responsive to some, but not all inhibitors. To address this, we examined the 3658 singly phosphorylated sites where effects of all four inhibitors could be quantified, looking for cases where the phosphosites were responsive to at least one, but not all four inhibitors [identified using a threshold of $|\log_2(\text{combined ratio})| \geq 0.84$, corresponding to z-scores less than -3.1 or greater than 3.1], while being clearly unresponsive to the remaining inhibitors [identified using a threshold of $|\log_2(\text{combined ratio})| \leq 0.30$, corresponding to z-scores between -1.1 and 1.1]. Of the phosphosites significantly responsive to at least one inhibitor, none were responsive only to the MKK1/2 inhibitors (trametinib and selumetinib), or only to the ERK1/2 inhibitors (SCH772984 and GDC0994) (Fig. 5*A*, supplemental Fig. S5). The significance of this null outcome is that branchpoints representing targets of MKK1/2 that bifurcate upstream of ERK1/2 would yield phosphosites responsive to MKK1/2 inhibitors but not ERK1/2 inhibitors. Therefore, we find no evidence of pathway bifurcation at the level of MKK1/2, upstream of ERK1/2. The absence of this pattern in a large data set reinforces the conclusion that kinases in the MAPK pathway mostly signal in a linear manner.

Special attention was paid to phosphosites that were significantly responsive to only one inhibitor [$|\log_2(\text{combined ratio})| \geq 0.84$], but clearly nonresponsive to the other three inhibitors [$|\log_2(\text{combined ratio})| \leq 0.3$] (Fig. 5*A*). We identified 21 cases of sites uniquely regulated by each inhibitor (Fig. 5*A*). These represent candidates for off-targets of each compound, as in the case of trametinib and p38α. Strikingly, 17 of the 21 phosphosites were uniquely responsive to GDC0994. This could not be explained by differential inhibition of ERK1/2 signaling by GDC0994, given that all four compounds strongly blocked phosphorylation of the ERK1/2 target, pp90RSK (supplemental Fig. S2). Thus, by comparing many inhibitors that target the same linear pathway, we can evaluate each individual compound for potential off-target effects, reflected by phosphosites which respond to only one inhibitor.

The candidates for off-target phosphosites are listed in Table II. Off-target sites for GDC0994 were found on proteins associated with RNA processing, including the pre-mRNA splicing protein, GEMIN7, the mRNA binding and translation regulator, LARP1B, and the poly(A) and mRNA cap binding protein, EIF4G1. Off-targets were also found on GTPase-associated proteins, including the G protein suppressor, GPS1, and the Rac binding and actin remodeling protein, BAIAP2L1. Thus, off-target responses to GDC0994 might be found with cellular events related to splicing, translation, or GTPase regulation. A potentially important off-target was Thr509 on dihydropyrimidinase-like 2 and 3 (DPYSL2 and DPYSL3, *aka* collapsin response mediator proteins, CRMP2 and CRMP4), which mediate neurite formation and whose expression is increased in liver, pancreatic, and neuroblastoma cancers (52–54). DPYSL2/3-Thr509 is phosphorylated by GSK3β, and phosphorylation is known to regulate protein-protein interactions (55, 56). Our findings illustrate the strategy of comparing many inhibitors of the same pathway by phosphoproteomics, to provide insight into the promiscuity of kinase inhibitors which may ultimately impact their clinical behavior.

Finally, we examined phosphosites that failed to respond to any MKK1/2 or ERK1/2 inhibitor. In total, 1649 Ser/Thr-Pro phosphorylation sites were completely unresponsive to MAPK pathway signaling, based on $\log_2(\text{ratio}) \geq -0.30$ with all four inhibitors (supplemental Table S6). Yet among this set, 45 matched the database of known ERK1/2 targets (supplemental Tables S6, S7). Therefore, several proteins which have been validated as direct targets of ERK1/2 in other cell systems are unambiguously insensitive to ERK1/2 in our system. Examples included Ser365 (originally numbered Ser323) on telomeric repeat binding factor (TERF2, *aka* TRF2), which in A375 cells is phosphorylated by ERK, increasing the protein half-life and promoting telomere protection and length stability (57). In addition, phosphorylation of Ser575 on stromal interaction molecule 1 (STIM1) by ERK is required for store operated calcium entry, promoting migration in endometrial adenocarcinoma cells and myogenesis in C2C12 myoblasts (58–60). The results demonstrate that canonical phosphoproteomic responses to the MAPK pathway can be variable depending on the cell system used, allowing some phosphorylation targets to be consistently regulated, but others to be bypassed.

TABLE II
Phosphorylation sites responsive to only one MKK1/2 or ERK1/2 inhibitor

Uniprot ID	Gene name	Protein name	Position	TRA/DMSO[a]	SEL/DMSO[a]	SCH/DMSO[a]	GDC/DMSO[a]
Q86UE4	MTDH	Protein LYRIC	S298	**−1.004**	−0.066	−0.019	0.250
Q15154	PCM1	Pericentriolar material 1 protein	S93	**−0.88**	−0.01	0.19	0.58
P10071	GLI3	Transcriptional activator/repressor	S445	−0.17	**−2.07**	−0.18	−0.23
P38159	RBMX	RNA-binding motif protein, X chr.	S88	−0.061	−0.112	**−0.952**	−0.096
Q04637	EIF4G1	Eukaryotic translation initiat. factor 4 γ1	S1209	0.335	0.215	−0.146	**−2.659**
Q16555	DPYSL2	Dihydropyrimidinase-related prot. 2	T509	0.234	0.229	0.046	**−1.561**
Q14195	DPYSL3	Dihydropyrimidinase-related prot. 3	T509	0.33	0.243	0.097	**−1.370**
Q03252	LMNB2	Lamin-B2	S17	−0.26	0.03	−0.28	**−1.41**
Q13098	GPS1	COP9 signalosome subunit 1	T479	−0.026	0.173	0.064	**−1.277**
Q68DQ2	CRYBG3	Very large A-kinase anchor protein	T2902	−0.055	0.115	0.108	**−1.275**
Q659C4	LARP1B	La-related protein 1B	S900	0.098	0.161	0.186	**−1.077**
Q9H840	GEMIN7	Gem-associated protein 7	T3	0.295	0.229	0.272	**−1.015**
O14777	NDC80	Kinetochore prot. NDC80 homolog	S69	−0.134	0.319	0.115	**−0.902**
Q6Y7W6	GIGYF2	PERQ aa-rich with GYF protein 2	S189	−0.051	0.183	−0.107	**−0.902**
P08034	GJB1	Gap junction beta-1 protein	S266	−0.043	−0.079	−0.065	**−0.872**
Q8NCF5	NFATC2IP	NFATC2-interacting protein	S84	0.357	0.249	0.081	**−0.865**
Q8NDD1	C1orf131	Uncharacterized protein C1orf131	S280	−0.026	0.161	−0.019	**−0.850**
Q9UHR4	BAIAP2L1	Brain angiogenesis inhibitor 1–2-like 1	S261	−0.104	−0.451	−0.063	**0.883**[b]
Q8WUZ0	BCL7C	B-cell CLL/lymphoma 7 family mem. C	S126	−0.425	−0.595	−0.126	**0.898**[b]
Q09666	AHNAK	Neuroblast differentiation assoc. prot	T4564	−0.211	0.252	−0.453	**0.995**[b]
P19532	TFE3	Transcription factor E3	S548	−0.194	−0.045	0.104	**1.045**[b]

[a] Empirical Bayes-generated $\log_2$(combined ratio) ($n \geq 2$) of SILAC replicates for each experiment.
[b] Four phosphosites were significantly increased in response to only one inhibitor.

DISCUSSION

Our study uses phosphoproteomics to compare molecular responses to inhibitors which target protein kinases in multiple tiers of the MAPK cascade in a single cell system. In doing so, we gain valuable insight into oncogenic BRAF signaling behavior in melanoma cells, as well as new information about MAPK pathway organization, specificity of phosphorylation, and off-target responses to therapeutics that are used in clinic or are under development. Four main conclusions can be reached from the findings in this study:

First, the phosphosites that are significantly regulated by MKK1/2 and ERK1/2 inhibitors show a high degree of overlap. We observed no responses that were unique to only MKK1/2 or only ERK1/2 inhibitors. This suggests that the signaling pathway is mostly devoid of targets for MKK1/2 that bifurcate upstream of ERK1/2. A previous study from our lab showed similar behavior upon comparing the BRAF inhibitor, vemurafenib, to the MKK1/2 inhibitor, selumetinib. Together our findings show little evidence for bifurcation in the pathway, and instead indicate that signaling downstream of oncogenic BRAF involves a linear organization of protein kinases, from BRAF to MKK1/2, and from MKK1/2 to ERK1/2.

Second, our study allowed us to identify phosphorylation sites most likely to be *bona fide* targets of the MAPK pathway, revealed by the 161 sites significantly regulated by all four MKK1/2 and ERK1/2 inhibitors. Importantly, dozens of phosphosites were implicated as potentially novel targets of ERK. Of the 103 phosphosites with Ser/Thr-Pro sequence specificity for ERK, only 20% matched known ERK targets, suggesting 82 potential new targets for direct phosphorylation. By searching for identifiers of MAPK substrates, including proximity to Pro at position P-2 and the presence of DEF or DEJL docking motifs, a subset of 47 phosphosites were prioritized as likely substrates of ERK1/2 that were previously unreported (Table I). The significance of this analysis is that, even though more than 700 sites for phosphorylation by ERK have been described *in vitro* and/or *in vivo*, the number that remain to be discovered is still unknown. Using phosphoproteomics to identify new substrates is hindered by an incomplete knowledge of inhibitor specificity for kinases, as well as the possibility of off-target effects. However, under conditions where a pathway signals in a linear fashion, as appears to be the case with the enzymes in the MAPK pathway, comparing the coordinate effects of multiple inhibitors toward more than one tier of the kinase cascade, together with sequence determinants of ERK substrates, provides a stringent filter for specificity. The results suggest that new types of cellular processes are regulated by ERK1/2, and expands our knowledge of the pleiotropy of cellular responses that may be affected by this essential signaling kinase.

Third, we showed that, of the phosphosites found to significantly respond to at least one of four kinase inhibitors, 21 sites responded to only one compound and were clearly unresponsive to the other three. This provides an effective filter to identify inhibitor off-target effects. Interestingly, most of the unambiguous off-target phosphosites responded to the ERK1/2 inhibitor, GDC0994, whereas those for other kinase inhibitors were relatively few. This may be important to consider when evaluating ERK1/2 inhibitors as tools to overcome resistance to BRAF and MKK1/2 inhibitor combinations. Even a single off-target can be meaningful, as suggested by the inhibition of MKK6 by the clinically relevant MKK1/2 inhibitor

trametinib. Blocking the p38α MAPK pathway can affect survival by promoting oncogenic or tumor suppressive effects, depending on cell type or stimulation. Although the IC_{50} for p38α MAPK inhibition by trametinib was high compared with MKK1/2-ERK1/2, this concentration range is often used in literature studies. We found that the p38 MAPK inhibitor, SB203580, augmented the cell inhibitory response to selumetinib, suggesting that inhibiting p38 synergizes with MKK1/2 inhibitors in melanoma cell lines to compromise cell viability. The behavior is consistent with reports showing a protective effect of CA-MKK6 and p38 MAPK signaling against UV-induced apoptosis in melanoma cells (61). The synergistic effect was muted when SB203580 was used in combination with trametinib, which we propose is because of the off-target effect of trametinib on MKK6. The results suggest that the effect of trametinib on p38α MAPK may augment the efficacy of this drug under certain conditions.

Finally, we addressed the issue of differential regulation of phosphorylation targets downstream of BRAF-MKK-ERK signaling. Different proteomics studies often show variations in phosphosite responses to the same pathway, but cannot distinguish whether such effects are because of differential signaling responses or experimental variability. Stuart *et al.* (5) compared phosphoproteomic responses to MKK1/2 inhibitors reported by several lab by analyzing only those phosphosites quantified in all experiments. The outcomes showed evidence for differential responses to the same pathway in different cell systems. However, the analysis could not exclude the possibility that experimental variations between laboratories or off-target effects of inhibitors could explain some of the observed differences. Our comparison of four inhibitors using data collected by one lab in one cell system allowed us to re-address this question more rigorously. We show conclusively that some, but not all, validated targets of ERK1/2 avoid phosphorylation in our cell system. The importance of this finding is that very little is understood about why some phosphorylation sites which are normally regulated by ERK are bypassed under certain conditions, whereas others are consistently targeted. The underlying mechanisms that lead to differential regulation within the phosphoproteome may be key to understanding the processes that control variability in cellular responses.

In conclusion, by comparing multiple inhibitors of multiple kinase tiers using phosphoproteomics, we gain new insight into new targets for regulation by the oncogenic BRAF driver pathway in cancer cells, and a useful approach for evaluating the specificity of drugs and drug candidates.

DATA AVAILABILITY

The mass spectrometry proteomics data have been deposited to the ProteomeXchange Consortium (10) via the PRIDE partner repository with the data set identifiers PXD007620 (DMSO-trametinib-SCH772984 SILAC experiment), PXD001560 (DMSO-selumetinib-vemurafenib SILAC experiment), and PXD007621 (DMSO-SCH772984-GDC0994 SILAC experiment).

* This study was funded by NIH R01 GM114594 (N.G.A.), NIH T32 GM007135 (J.B.), ACS PF-11-071-01-TBG (S.A.S.), NSF-IGERT 1144807 (A.J.K.), and DARPA 13-34-RTA-FP-007 (W.M.O.).

[S] This article contains supplemental material.

‖ To whom correspondence should be addressed: Department of Chemistry and Biochemistry, BioFrontiers Institute, University of Colorado, Boulder, CO 80303. Tel.: 303.492.4799; Fax: 303.492.8425; E-mail: natalie.ahn@colorado.edu.

REFERENCES

1. Burotto, M., Chiou, V. L., Lee, J.-M., and Kohn, E. C. (2014) The MAPK pathway across different malignancies: a new perspective. *Cancer* **120,** 3446–3456
2. Flaherty, K. T., Hodi, F. S., and Fisher, D. E. (2012) From genes to drugs: targeted strategies for melanoma. *Nat. Rev. Cancer* **12,** 349–361
3. Wu, P., Nielsen, T. E., and Clausen, M. H. (2015) FDA-approved small-molecule kinase inhibitors. *Trends Pharmacol. Sci.* **36,** 422–439
4. Signorelli, J., and Shah Gandhi, A. (2017) Cobimetinib. *Ann. Pharmacother.* **51,** 146–153
5. Stuart Sa. Houel, S., Lee, T., Wang, N., Old, W. M., and Ahn, N. G. (2015) A phosphoproteomic comparison of B-RAFV600E and MKK1/2 inhibitors in melanoma cells. *Mol. Cell. Proteomics* **14,** 1599–1615
6. Van Allen, E. M., Wagle, N., Sucker, A., Treacy, D. J., Johannessen, C. M., Goetz, E. M., Place, C. S., Taylor-Weiner, A., Whittaker, S., Kryukov, G. V., Hodis, E., Rosenberg, M., McKenna, A., Cibulskis, K., Farlow, D., Zimmer, L., Hillen, U., Gutzmer, R., Goldinger, S. M., Ugurel, S., Gogas, H. J., Egberts, F., Berking, C., Trefzer, U., Loquai, C., Weide, B., Hassel, J. C., Gabriel, S. B., Carter, S. L., Getz, G., Garraway, L. A., Schadendorf, D., and Dermatologic Cooperative Oncology Group of Germany (DeCOG). (2014) The genetic landscape of clinical resistance to RAF inhibition in metastatic melanoma. *Cancer Discov.* **4,** 94–109
7. Morris, E. J., Jha, S., Restaino, C. R., Dayananth, P., Zhu, H., Cooper, A., Carr, D., Deng, Y., Jin, W., Black, S., Long, B., Liu, J., Dinunzio, E., Windsor, W., Zhang, R., Zhao, S., Angagaw, M. H., Pinheiro, E. M., Desai, J., Xiao, L., Shipps, G., Hruza, A., Wang, J., Kelly, J., Paliwal, S., Gao, X., Babu, B. S., Zhu, L., Daublain, P., Zhang, L., Lutterbach, B. A., Pelletier, M. R., Philippar, U., Siliphaivanh, P., Witter, D., Kirschmeier, P., Bishop, W. R., Hicklin, D., Gilliland, D. G., Jayaraman, L., Zawel, L., Fawell, S., and Samatar, A. A. (2013) Discovery of a novel ERK inhibitor with activity in models of acquired resistance to BRAF and MEK inhibitors. *Cancer Discov.* **3,** 742–750
8. Blake, J. F., Burkard, M., Chan, J., Chen, H., Chou, K.-J., Diaz, D., Dudley, D. A., Gaudino, J. J., Gould, S. E., Grina, J., Hunsaker, T., Liu, L., Martinson, M., Moreno, D., Mueller, L., Orr, C., Pacheco, P., Qin, A., Rasor, K., Ren, L., Robarge, K., Shahidi-Latham, S., Stults, J., Sullivan, F., Wang, W., Yin, J., Zhou, A., Belvin, M., Merchant, M., Moffat, J., and Schwarz, J. B. (2016) Discovery of (S)-1-(1-(4-Chloro-3-fluorophenyl)-2-hydroxyethyl)-4-(2-((1-methyl-1H-pyrazol-5-yl)amino)pyrimidin-4-yl)pyridin-2(1H)-one (GDC-0994), an extracellular signal-regulated kinase 1/2 (ERK1/2) inhibitor in early clinical development. *J. Med. Chem.* **59,** 5650–5660
9. Cox, J., and Mann, M. (2008) MaxQuant enables high peptide identification rates, individualized p.p.b.-range mass accuracies and proteome-wide protein quantification. *Nat. Biotechnol.* **26,** 1367–1372
10. Vizcaíno, J. A., Deutsch, E. W., Wang, R., Csordas, A., Reisinger, F., Ríos, D., Dianes, J. A., Sun, Z., Farrah, T., Bandeira, N., Binz, P.-A., Xenarios, I., Eisenacher, M., Mayer, G., Gatto, L., Campos, A., Chalkley, R. J., Kraus, H.-J., Albar, J. P., Martinez-Bartolomé, S., Apweiler, R., Omenn, G. S., Martens, L., Jones, A. R., and Hermjakob, H. (2014) ProteomeXchange provides globally coordinated proteomics data submission and dissemination. *Nat. Biotechnol.* **32,** 223–226
11. Ritchie, M. E., Phipson, B., Wu, D., Hu, Y., Law, C. W., Shi, W., and Smyth, G. K. (2015) Limma powers differential expression analyses for RNA-sequencing and microarray studies. *Nucleic Acids Res.* **43,** e47
12. Poss, Z. C., Ebmeier, C. C., Odell, A. T., Tangpeerachaikul, A., Lee, T., Pelish, H. E., Shair, M. D., Dowell, R. D., Old, W. M., and Taatjes, D. J. (2016) Identification of mediator kinase substrates in human cells using

cortistatin A and quantitative phosphoproteomics. *Cell Rep.* **15,** 436–450
13. Margolin, A. A., Ong, S.-E., Schenone, M., Gould, R., Schreiber, S. L., Carr, S. A., and Golub, T. R. (2009) Empirical Bayes analysis of quantitative proteomics experiments. *PLoS ONE* **4,** e7454
14. Raingeaud, J., Whitmarsh, A. J., Barrett, T., Dérijard, B., and Davis, R. J. (1996) MKK3- and MKK6-regulated gene expression is mediated by the p38 mitogen-activated protein kinase signal transduction pathway. *Mol. Cell. Biol.* **16,** 1247–1255
15. Sours, K. M., Xiao, Y., and Ahn, N. G. (2014) Extracellular-regulated kinase 2 is activated by the enhancement of hinge flexibility. *J. Mol. Biol.* **426,** 1925–1935
16. Zarei, M., Sprenger, A., Gretzmeier, C., and Dengjel, J. (2013) Rapid combinatorial ERLIC-SCX solid-phase extraction for in-depth phosphoproteome analysis. *J. Proteome Res.* **12,** 5989–5895
17. Wiśniewski, J. R., Zougman, A., Nagaraj, N., and Mann, M. (2009) Universal sample preparation method for proteome analysis. *Nat. Methods* **6,** 359–362
18. Olsen, J. V., Blagoev, B., Gnad, F., Macek, B., Kumar, C., Mortensen, P., and Mann, M. (2006) Global, in vivo, and site-specific phosphorylation dynamics in signaling networks. *Cell* **127,** 635–648
19. Basbous, J., Chalbos, D., Hipskind, R., Jariel-Encontre, I., and Piechaczyk, M. (2007) Ubiquitin-independent proteasomal degradation of Fra-1 is antagonized by Erk1/2 pathway-mediated phosphorylation of a unique C-terminal destabilizer. *Mol. Cell. Biol.* **27,** 3936–3950
20. Chaikuad, A., Tacconi, E. M. C., Zimmer, J., Liang, Y., Gray, N. S., Tarsounas, M., and Knapp, S. (2014) A unique inhibitor binding site in ERK1/2 is associated with slow binding kinetics. *Nat. Chem. Biol.* **10,** 853–860
21. Flaherty, K. T., Infante, J. R., Daud, A., Gonzalez, R., Kefford, R. F., Sosman, J., Hamid, O., Schuchter, L., Cebon, J., Ibrahim, N., Kudchadkar, R., Burris, H. A., Falchook, G., Algazi, A., Lewis, K., Long, G. V., Puzanov, I., Lebowitz, P., Singh, A., Little, S., Sun, P., Allred, A., Ouellet, D., Kim, K. B., Patel, K., and Weber, J. (2012) Combined BRAF and MEK inhibition in melanoma with BRAF V600 mutations. *N. Engl. J. Med.* **367,** 1694–1703
22. Cuenda, A., and Rousseau, S. (2007) p38 MAP-kinases pathway regulation, function and role in human diseases. *Biochim. Biophys. Acta* **1773,** 1358–1375
23. Zarubin, T., and Han, J. (2005) Activation and signaling of the p38 MAP kinase pathway. *Cell Res.* **15,** 11–18
24. Zhou, Y., Tanaka, T., Sugiyama, N., Yokoyama, S., Kawasaki, Y., Sakuma, T., Ishihama, Y., Saiki, I., and Sakurai, H. (2014) p38-Mediated phosphor-
ylation of Eps15 endocytic adaptor protein. *FEBS Lett.* **588,** 131–137
25. Mavrogonatou, E., and Kletsas, D. (2009) High osmolality activates the G1 and G2 cell cycle checkpoints and affects the DNA integrity of nucleus pulposus intervertebral disc cells triggering an enhanced DNA repair response. *DNA Repair* **8,** 930–943
26. Mavrogonatou, E., and Kletsas, D. (2012) Differential response of nucleus pulposus intervertebral disc cells to high salt, sorbitol, and urea. *J. Cell. Physiol.* **227,** 1179–1187
27. Yamaguchi, T., Kakefuda, R., Tajima, N., Sowa, Y., and Sakai, T. (2011) Antitumor activities of JTP-74057 (GSK1120212), a novel MEK1/2 inhibitor, on colorectal cancer cell lines in vitro and in vivo. *Int. J. Oncol.* **39,** 23–31
28. Infante, J. R., Fecher, L. A., Falchook, G. S., Nallapareddy, S., Gordon, M. S., Becerra, C., DeMarini, D. J., Cox, D. S., Xu, Y., Morris, S. R., Peddareddigari, V. G. R., Le, N. T., Hart, L., Bendell, J. C., Eckhardt, G., Kurzrock, R., Flaherty, K., Burris, H. A., and Messersmith, W. A. (2012) Safety, pharmacokinetic, pharmacodynamic, and efficacy data for the oral MEK inhibitor trametinib: a phase 1 dose-escalation trial. *Lancet. Oncol.* **13,** 773–781
29. Uitdehaag, J. C. M., de Roos, J. A. D. M., van Doornmalen, A. M., Prinsen, M. B. W., de Man, J., Tanizawa, Y., Kawase, Y., Yoshino, K., Buijsman, R. C., and Zaman, G. J. R. (2014) Comparison of the cancer gene targeting and biochemical selectivities of all targeted kinase inhibitors approved for clinical use. *PLoS ONE* **9,** e92146
30. Ohren, J. F., Chen, H., Pavlovsky, A., Whitehead, C., Zhang, E., Kuffa, P., Yan, C., McConnell, P., Spessard, C., Banotai, C., Mueller, W. T., Delaney, A., Omer, C., Sebolt-Leopold, J., Dudley, D. T., Leung, I. K., Flamme, C., Warmus, J., Kaufman, M., Barrett, S., Tecle, H., and Hasemann, C. A. (2004) Structures of human MAP kinase kinase 1 (MEK1) and MEK2 describe novel noncompetitive kinase inhibition. *Nat. Struct. Mol. Biol.* **11,** 1192–1197
31. Robarge, K. D., Lee, W., Eigenbrot, C., Ultsch, M., Wiesmann, C., Heald, R., Price, S., Hewitt, J., Jackson, P., Savy, P., Burton, B., Choo, E. F., Pang, J., Boggs, J., Yang, A., Yang, X., and Baumgardner, M. (2014) Structure based design of novel 6,5 heterobicyclic mitogen-activated protein kinase kinase (MEK) inhibitors leading to the discovery of imidazo[1,5-a] pyrazine G-479. *Bioorg. Med. Chem. Lett.* **24,** 4714–4723
32. Rudolph, J., Xiao, Y., Pardi, A., and Ahn, N. G. (2015) Slow inhibition and conformation selective properties of extracellular signal-regulated kinase 1 and 2 inhibitors. *Biochemistry* **54,** 22–31
33. Ünal, EB, Uhlitz Fand Blüthgen, N. (2017) A compendium of ERK targets. *FEBS Lett.* **591,** 2607–2615
34. Yoon, S., and Seger, R. (2006) The extracellular signal-regulated kinase: multiple substrates regulate diverse cellular functions. *Growth Factors* **24,** 21–44
35. Xue, L., Wang, P., Cao, P., Zhu, J.-K., and Tao, W. A. (2014) Identification of extracellular signal-regulated kinase 1 (ERK1) direct substrates using stable isotope labeled kinase assay-linked phosphoproteomics. *Mol. Cell. Proteomics* **13,** 3199–3210
36. Carlson, S. M., Chouinard, C. R., Labadorf, A., Lam, C. J., Schmelzle, K., Fraenkel, E., and White, F. M. (2011) Large-scale discovery of ERK2 substrates identifies ERK-mediated transcriptional regulation by ETV3. *Sci. Signal.* **4,** rs11
37. Hornbeck, P. V., Zhang, B., Murray, B., Kornhauser, J. M., Latham, V., and Skrzypek, E. (2015) PhosphoSitePlus, 2014: mutations, PTMs and recalibrations. *Nucleic Acids Res.* **43,** D512–D520
38. Chung, J., Uchida, E., Grammer, T. C., and Blenis, J. (1997) STAT3 serine phosphorylation by ERK-dependent and -independent pathways negatively modulates its tyrosine phosphorylation. *Mol. Cell. Biol.* **17,** 6508–6516
39. Srsen, V., Kitazawa, H., Sugita, M., Murofushi, H., Bulinski, J. C., Kishimoto, T., and Hisanaga, S. (1999) Serum-dependent phosphorylation of human MAP4 at Ser696 in cultured mammalian cells. *Cell Struct. Funct.* **24,** 321–327
40. Kubiniok, P., Lavoie, H., Therrien, M., and Thibault, P. (2017) Time-resolved Phosphoproteome Analysis of Paradoxical RAF Activation Reveals Novel Targets of ERK. *Mol. Cell. Proteomics* **16,** 663–679
41. Davis, R. J. (1993) The mitogen-activated protein kinase signal transduction pathway. *J. Biol. Chem.* **268,** 14553–14556
42. Cargnello, M., and Roux, P. P. (2011) Activation and function of the MAPKs and their substrates, the MAPK-activated protein kinases. *Microbiol. Mol. Biol. Rev.* **75,** 50–83
43. Roskoski, R. (2012) ERK1/2 MAP kinases: structure, function, and regulation. *Pharmacol. Res.* **66,** 105–143
44. Piserchio, A., Warthaka, M., Kaoud, T. S., Callaway, K., Dalby, K. N., and Ghose, R. (2017) Local destabilization, rigid body, and fuzzy docking facilitate the phosphorylation of the transcription factor Ets-1 by the mitogen-activated protein kinase ERK2. *Proc. Natl. Acad. Sci. U.S.A.* **114,** E6287–E6296
45. Piserchio, A., Francis, D. M., Koveal, D., Dalby, K. N., Page, R., Peti, W., and Ghose, R. (2012) Docking interactions of hematopoietic tyrosine phosphatase with MAP kinases ERK2 and p38α. *Biochemistry* **51,** 8047–8049
46. Garai Á., Zeke, A., Gógl, G., Törő, I., Fördős, F., Blankenburg, H., Bárkai, T., Varga, J., Alexa, A., Emig, D., Albrecht, M., and Reményi, A. (2012) Specificity of linear motifs that bind to a common mitogen-activated protein kinase docking groove. *Sci. Signal.* **5,** ra74
47. Zeke, A., Bastys, T., Alexa, A., Garai Á Mészáros. B, Kirsch, K., Dosztányi, Z., Kalinina, O. V., and Reményi, A. (2015) Systematic discovery of linear binding motifs targeting an ancient protein interaction surface on MAP kinases. *Mol. Syst. Biol.* **11,** 837
48. Obenauer, J. C., Cantley, L. C., and Yaffe, M. B. (2003) Scansite 2.0: Proteome-wide prediction of cell signaling interactions using short sequence motifs. *Nucleic Acids Res.* **31,** 3635–3641
49. Spilker, C., and Kreutz, M. R. (2010) RapGAPs in brain: multipurpose players in neuronal Rap signalling. *Eur. J. Neurosci.* **32,** 1–9
50. Huang, D. W., Sherman, B. T., and Lempicki, R. A. (2009) Systematic and integrative analysis of large gene lists using DAVID bioinformatics resources. *Nat. Protoc.* **4,** 44–57
51. Hömig-Hölzel, C., van Doorn, R., Vogel, C., Germann, M., Cecchini, M. G., Verdegaal, E., and Peeper, D. S. (2011) Antagonistic TSC22D1 variants control BRAF(E600)-induced senescence. *EMBO J.* **30,** 1753–1765

52. Hiroshima, Y., Nakamura, F., Miyamoto, H., Mori, R., Taniguchi, K., Matsuyama, R., Akiyama, H., Tanaka, K., Ichikawa, Y., Kato, S., Kobayashi, N., Kubota, K., Nagashima, Y., Goshima, Y., and Endo, I. (2013) Collapsin response mediator protein 4 expression is associated with liver metastasis and poor survival in pancreatic cancer. *Ann. Surg. Oncol.* **20,** S369–S378
53. Kawahara, T., Hotta, N., Ozawa, Y., Kato, S., Kano, K., Yokoyama, Y., Nagino, M., Takahashi, T., and Yanagisawa, K. (2013) Quantitative proteomic profiling identifies DPYSL3 as pancreatic ductal adenocarcinoma-associated molecule that regulates cell adhesion and migration by stabilization of focal adhesion complex. *PLoS ONE* **8,** e79654
54. Tan, F., Wahdan-Alaswad, R., Yan, S., Thiele, C. J., and Li, Z. (2013) Dihydropyrimidinase-like protein 3 expression is negatively regulated by MYCN and associated with clinical outcome in neuroblastoma. *Cancer Sci.* **104,** 1586–1592
55. Cole, A. R., Causeret, F., Yadirgi, G., Hastie, C. J., McLauchlan, H., McManus, E. J., Hernández, F., Eickholt, B. J., Nikolic, M., and Sutherland, C. (2006) Distinct priming kinases contribute to differential regulation of collapsin response mediator proteins by glycogen synthase kinase-3 in vivo. *J. Biol. Chem.* **281,** 16591–16598
56. Mizuno, M., Kato, D., Kanamori, T., Toyoda, T., Suzuki, T., Ojika, K., and Matsukawa, N. (2013) Phosphorylation of collapsin response mediator protein-2 regulates its localization and association with hippocampal cholinergic neurostimulating peptide precursor in the hippocampus. *Neurosci. Lett.* **535,** 122–127
57. Picco, V., Coste, I., Giraud-Panis, M.-J., Renno, T., Gilson, E., and Pagès, G. (2016) ERK1/2/MAPK pathway-dependent regulation of the telomeric factor TRF2. *Oncotarget* **7,** 46615–46627
58. Pozo-Guisado, E., Casas-Rua, V., Tomas-Martin, P., Lopez-Guerrero, A. M., Alvarez-Barrientos, A., and Martin-Romero, F. J. (2013) Phosphorylation of STIM1 at ERK1/2 target sites regulates interaction with the microtubule plus-end binding protein EB1. *J. Cell Sci.* **126,** 3170–3180
59. Casas-Rua, V., Tomas-Martin, P., Lopez-Guerrero, A. M., Alvarez, I. S., Pozo-Guisado, E., and Martin-Romero, F. J. (2015) STIM1 phosphorylation triggered by epidermal growth factor mediates cell migration. *Biochim. Biophys. Acta* **1853,** 233–243
60. Lee, H.-J., Bae, G.-U., Leem, Y.-E., Choi, H.-K., Kang, T. M., Cho, H., Kim, S.-T., and Kang, J.-S. (2012) Phosphorylation of Stim1 at serine 575 via netrin-2/Cdo-activated ERK1/2 is critical for the promyogenic function of Stim1. *Mol. Biol. Cell* **23,** 1376–1387
61. Ivanov, V. N., and Ronai, Z. (2000) p38 protects human melanoma cells from UV-induced apoptosis through down-regulation of NF-kappaB activity and Fas expression. *Oncogene* **19,** 3003–3012